GALACTIC GLOBULAR CLUSTER RELATIVE AGES[1]

A. ROSENBERG

Telescopio Nazionale Galileo, Osservatorio Astronomico di Padova, vicolo dell'Osservatorio 5, I-35122 Padova, Italy; rosenberg@pd.astro.it

I. SAVIANE AND G. PIOTTO

Dipartimento di Astronomia, Università di Padova, vicolo dell'Osservatorio 5, I-35122 Padova, Italy; saviane@pd.astro.it, piotto@pd.astro.it

AND

A. APARICIO

Instituto de Astrofísica de Canarias, Via Lactea, E-38200 La Laguna, Tenerife, Spain; aaj@iac.es

ABSTRACT

Based on a new large, homogeneous photometric database of 34 Galactic globular clusters (GGCs; plus Palomar 12), a set of distance- and reddening- independent relative age indicators has been measured. The observed $\delta(V-I)_{2.5}$ and ΔV_{TO}^{HB} versus metallicity relations have been compared with the relations predicted by two recently updated libraries of isochrones. Using these models and two independent methods, we have found that self-consistent relative ages can be estimated for our GGC sample. In turn, this demonstrates that the models are internally self-consistent. Based on the relative age versus metallicity distribution, we conclude that (1) there is no evidence of an age spread for clusters with [Fe/H] < -1.2, all the clusters of our sample in this range being old and coeval; (2) for the intermediate-metallicity group ($-1.2 \leq$ [Fe/H] < -0.9), there is a clear evidence of age dispersion, with clusters up to $\sim 25\%$ younger than the older members; and (3) the clusters within the metal-rich group ([Fe/H] ≥ -0.9) seem to be coeval within the uncertainties (except Pal 12) but younger ($\sim 17\%$) than the bulk of the GGCs. The latter result is totally model dependent. From the Galactocentric distribution of the GGC ages, we can divide the GGCs in two groups: the old, coeval clusters and the young clusters. The second group can be divided into two subgroups: the "really young clusters" and the "young, but model dependent," which are within the intermediate- and high-metallicity groups, respectively. From this distribution, we can present a possible scenario for the Milky Way's formation: The globular cluster formation process started at the same zero age throughout the halo, at least out to ~ 20 kpc from the Galactic center. According to the present stellar evolution models, the metal-rich clusters are formed at a later time ($\sim 17\%$ lower age). Finally, significantly younger halo GGCs are found at any $R_{GC} > 8$ kpc. For these, a possible scenario associated with mergers of dwarf galaxies to the Milky Way is suggested.

Key words: color-magnitude diagrams — Galaxy: evolution — Galaxy: formation — globular clusters: general — stars: Population II

1. INTRODUCTION

Galactic globular clusters (GGCs) are the oldest components of the Galactic halo for which ages can be obtained. The determination of their relative ages and of any age correlation with metallicities, abundance patterns, positions, and kinematics provides clues to the formation timescale of the halo and provides information on the early efficiency of the enrichment processes in the proto-Galactic material. The importance of these problems and the difficulty in answering these questions is at the basis of the huge efforts dedicated to gather the relative ages of GGCs in the last 30 years or so (VandenBerg, Stetson, & Bolte 1996 and references therein; Sarajedini, Chaboyer, & Demarque 1997 and references therein).

The methods used for the age determination of GGCs are based on the position of the turnoff (TO) in the color-magnitude diagram (CMD) of their stellar population. We can measure either the absolute magnitude or the dereddened color of the TO. However, in order to overcome the uncertainties intrinsic to any method of obtaining GGC distances and reddening, it is common to measure either the color or the magnitude (or both) of the TO, relative to some other point in the CMD whose position has a negligible dependence on age.

Observationally, as pointed out by Sarajedini & Demarque (1990, hereafter SD90) and VandenBerg, Bolte, & Stetson (1990, hereafter V90), the most precise relative-age indicator is based on the TO color relative to some fixed point on the red giant branch (RGB). This is usually called the "horizontal method." Unfortunately, the theoretical RGB temperature is very sensitive to the adopted mixing-length parameter, whose dependence on metallicity is not yet well established. As a consequence, investigations of relative ages based on the horizontal method might be of difficult interpretation and need a careful calibration of the relative TO color as a function of the relative age (Buonanno et al. 1998, hereafter B98). The other age indicator, the "vertical method," is based on the TO luminosity relative to the horizontal branch (HB). Though this is usually considered a more robust relative-age indicator, it is affected both by the uncertainty of the dependence of the

HB luminosity on metallicity and the empirical difficulties to obtain the TO and by the HB magnitudes for clusters with only blue HBs. It has also been pointed out by Sweigart (1997) and Sandquist et al. (1999) that there is the possibility that, at a given [Fe/H], there may be a dispersion in the content of helium in the envelope HB stars in different clusters. At a given [Fe/H], this would lead to a range in HB magnitude and add some scatter to the vertical method of relative-age determination. It must also be noted that both methods are affected by the still-uncertain dependence of the alpha elements and helium content on the metallicity.

Given these problems, it is still an open debate whether most GGCs are almost coeval (Stetson, VandenBerg, & Bolte 1996, hereafter S96) or whether there was a protracted formation epoch of 5 Gyr (Sarajedini et al. 1997) or so (i.e., for 30%–40% of the Galactic halo lifetime). Indeed, there is a major limitation to the large-scale GGC relative-age investigations: the photometric inhomogeneity and the inhomogeneity in the analysis of the databases used in the various studies. Many previous studies frequently combined photographic and CCD data or different databases (obtained with different instruments with uncertain calibrations to standard systems and/or based on different sets of standards), or inappropriate CMDs were used. This inhomogeneity affects even many recent works, for which results cannot yet been considered conclusive (see S96 for a discussion).

Recently, two new investigations have brought fresh views in this field. First, an analysis of published CMDs both in the B, V and V, I bands was carried out by Saviane, Rosenberg, & Piotto (1997, hereafter SRP97), who showed that the $V - I$ TO-RGB color differences are less sensitive to metallicity than the $B - V$ ones (while retaining the same age sensitivity). SRP97 also suggested that a high-precision, large-scale investigation in the V and I bands would have allowed a relative-age determination through the horizontal method without the usual limitation of dividing the clusters into different metallicity groups (V90). Still, a calibration of the horizontal methods in V and I was needed for a correct interpretation of the data. Later, B98 showed that, with an appropriate calibration based on the vertical method, reliable relative ages can indeed be obtained with the horizontal method. The investigation of B98 is based both on $B - V$ material from the literature and original data.

The results presented here take advantage of the strengths of both investigations. Soon after the SRP97 study, we began to collect homogeneous photometric material for a large sample of GGCs, in order to obtain accurate relative ages by using the horizontal method in the [Fe/H], $\delta(V - I)$ plane. Our first observational effort, aimed at the inner-to-intermediate halo clusters, is now complete, and we provide here the first results. In the next section, the data used for this study are presented. In § 3, we define our age indicators and explain how they have been measured on both the CMDs and theoretical models. Section 4 presents the measures obtained following this procedure and compares them with the predictions of the theoretical models. In § 5, we discuss our results. An analysis of the relative ages versus metallicity (§ 5.1) and Galactocentric distance (§ 5.3) is presented. The discussion also compares clusters in metallicity subgroups (§ 5.2). In § 6, the clues obtained until now are used to gather some information on the Milky

Way's formation and evolution. Finally, a summary is given in § 7. The potentiality of our database for testing the theoretical calculations is also discussed in Appendix B.

2. DATA

The goal of our observational strategy was to obtain color differences near the TO region with an uncertainty ≤ 0.01 mag, which allows a ≤ 1 Gyr age resolution. As a first step, we used 1 m–class telescopes to build a large reference sample, including all clusters within $(m - M)_V = 16$. The 91 cm ESO/Dutch Telescope (for the southern sky GGCs) and the 1 m Isaac Newton Group Jacobus Kapteyn Telescope (for the northern GGCs) were then used to cover 52 of the scheduled 69 clusters. Of the total sample, only 34 were suitable for this study. The remaining objects were excluded for several reasons: differential reddening, small number of member stars, large background contamination, and bad definition of the RGB or HB. One or two overlapping fields were covered for each cluster, avoiding the cluster center, especially when it is crowded. From 2500 to 20,000 stars per cluster were measured. The typical CMD extends from the RGB tip to ≥ 3 mag below the TO. The final selected sample is listed in Table 1. Cluster names are given in column (2). The assumed [Fe/H], which covers almost the entire GGC metallicity range $-2.1 \leq$ [Fe/H] ≤ -0.7, is given in column (3). The [Fe/H] values were taken (unless otherwise stated) from Rutledge, Hesser, & Stetson (1997; their Table 2, col. [6]). Column (4) lists the Galactocentric distance (from Harris 1996), which extends from 2 to ~ 20 kpc. The remaining columns report our measures, as discussed in § 4.

In our attempt to be as homogeneous as possible, we have adopted the metallicities listed in Rutledge et al. (1997). Their values were, in fact, obtained from a large and homogeneous work based on the Ca II triplet, and calibrated over both the Carretta & Gratton (1997) scale and the Zinn & West (1984) scale. In this paper, we adopt the Carretta & Gratton (1997) values, as their metallicity scale was obtained from high-resolution CCD spectra of 24 GGCs (20 in common with our sample), analyzed in a self-consistent way. The main results, presented in the following sections, would not change if we were to adopt the Zinn & West (1984) scale.

A detailed description of the observation and reduction strategies are given in Rosenberg et al. (1999a, 1999b, Papers I and II, respectively), where the CMDs for the whole photometric sample are also presented. Here, suffice it to say, the data have been calibrated with the same set of standards, and the absolute zero-point uncertainties of our calibrations are ≤ 0.02 mag for each of the two bands. Moreover, three clusters have been observed with both the southern and northern telescopes, thus providing a consistency check of the calibrations: the zero points are consistent within the calibration errors, and most importantly, no color term is found between the two data sets.

Only two well-known young clusters, Pal 1 (Rosenberg et al. 1998a) and Pal 12 (Rosenberg et al. 1998b, hereafter Paper III), have been observed in the V, I bands deep enough to allow the measurement of their TOs. Since Pal 1 has no HB stars, Pal 12 remains the only cluster that allows an extension of the present work to very young clusters; for this reason, it has been included in our analysis, even if its photometry is not strictly homogeneous (different equipment has been used) with that of the other clusters,

TABLE 1

Data for the 34 Analyzed GGCs and Pal 12

No. (1)	Cluster (2)	[Fe/H] (3)	R_{GC} (kpc) (4)	V_{TO} (5)	$(V-I)_{TO}$ (6)	V_{HB} (7)	ΔV_{TO}^{HB} (8)	$\delta(V-I)_{2.5}$ (9)
1	NGC 104	-0.78 ± 0.02	7.3	17.60 ± 0.08	0.660 ± 0.007	14.05 ± 0.05	3.55 ± 0.09	0.295 ± 0.010
2	NGC 288	-1.14 ± 0.03	11.4	18.90 ± 0.04	0.645 ± 0.002	15.40 ± 0.05	3.55 ± 0.06	0.276 ± 0.006
3	NGC 362	-1.09 ± 0.03	9.2	00.00 ± 0.09	0.000 ± 0.008	03.29 ± 0.05	3.29 ± 0.10	0.312 ± 0.011
4	NGC 1261	-1.08 ± 0.04	17.9	19.90 ± 0.06	0.555 ± 0.003	16.68 ± 0.05	3.22 ± 0.08	0.319 ± 0.007
5	NGC 1851	-1.03 ± 0.06	16.8	19.50 ± 0.07	0.630 ± 0.005	16.18 ± 0.05	3.32 ± 0.09	0.305 ± 0.008
6	NGC 1904	-1.37 ± 0.05	18.5	19.65 ± 0.09	0.610 ± 0.007	16.15 ± 0.05	3.50 ± 0.10	0.279 ± 0.010
7	NGC 2808	-1.11 ± 0.03	10.9	19.60 ± 0.07	0.800 ± 0.005	16.30 ± 0.05	3.30 ± 0.09	0.301 ± 0.008
8	NGC 3201	-1.24 ± 0.03	8.9	18.20 ± 0.05	0.905 ± 0.004	14.75 ± 0.05	3.45 ± 0.07	0.283 ± 0.008
9	NGC 4590	-2.00 ± 0.03	10.0	19.05 ± 0.07	0.605 ± 0.006	15.75 ± 0.10	3.30 ± 0.12	0.306 ± 0.010
10	NGC 5053	-1.98 ± 0.09	16.8	20.00 ± 0.06	0.545 ± 0.004	16.70 ± 0.05	3.30 ± 0.08	0.310 ± 0.007
11	NGC 5272	-1.33 ± 0.02^{a}	11.9	19.10 ± 0.04	0.575 ± 0.002	15.58 ± 0.05	3.52 ± 0.06	0.284 ± 0.005
12	NGC 5466	-2.13 ± 0.36^{b}	16.9	19.95 ± 0.07	0.555 ± 0.006	16.60 ± 0.05	3.35 ± 0.09	0.300 ± 0.009
13	NGC 5897	-1.73 ± 0.07	7.6	19.75 ± 0.07	0.720 ± 0.006	16.30 ± 0.10	3.45 ± 0.12	0.293 ± 0.011
14	NGC 5904	-1.12 ± 0.03	6.1	18.50 ± 0.03	0.625 ± 0.002	15.00 ± 0.05	3.50 ± 0.06	0.282 ± 0.005
15	NGC 6093	-1.47 ± 0.04	3.1	19.80 ± 0.08	0.815 ± 0.005	16.25 ± 0.05	3.55 ± 0.09	0.279 ± 0.009
16	NGC 6121	-1.05 ± 0.03	6.0	16.90 ± 0.03	1.125 ± 0.004	13.36 ± 0.05	3.54 ± 0.06	0.269 ± 0.007
17	NGC 6171	-0.95 ± 0.04	3.3	19.25 ± 0.06	1.150 ± 0.004	15.65 ± 0.05	3.60 ± 0.08	0.269 ± 0.007
18	NGC 6205	-1.33 ± 0.05	8.3	18.50 ± 0.06	0.575 ± 0.004	14.95 ± 0.10	3.55 ± 0.12	0.276 ± 0.009
19	NGC 6218	-1.14 ± 0.05	4.6	18.30 ± 0.07	0.850 ± 0.004	14.70 ± 0.10	3.60 ± 0.12	0.264 ± 0.010
20	NGC 6254	-1.25 ± 0.03	4.6	18.55 ± 0.05	0.930 ± 0.003	15.05 ± 0.10	3.50 ± 0.11	0.277 ± 0.009
21	NGC 6341	-2.10 ± 0.02^{a}	9.5	18.55 ± 0.06	0.555 ± 0.005	15.20 ± 0.10	3.35 ± 0.12	0.295 ± 0.010
22	NGC 6352	-0.70 ± 0.02	3.3	18.70 ± 0.07	0.985 ± 0.007	15.25 ± 0.05	3.45 ± 0.09	0.306 ± 0.010
23	NGC 6362	-0.99 ± 0.03	5.1	18.90 ± 0.08	0.685 ± 0.007	15.35 ± 0.05	3.55 ± 0.09	0.277 ± 0.010
24	NGC 6366	-0.73 ± 0.05	4.9	19.10 ± 0.06	1.570 ± 0.005	15.65 ± 0.05	3.45 ± 0.08	0.310 ± 0.009
25	NGC 6397	-1.76 ± 0.03	6.0	16.40 ± 0.04	0.775 ± 0.002	12.95 ± 0.10	3.45 ± 0.11	0.290 ± 0.008
26	NGC 6535	-1.51 ± 0.10	3.9	19.30 ± 0.06	1.105 ± 0.004	15.80 ± 0.10	3.50 ± 0.12	0.270 ± 0.010
27	NGC 6656	-1.41 ± 0.03^{a}	5.0	17.80 ± 0.07	0.960 ± 0.005	14.25 ± 0.10	3.55 ± 0.12	0.274 ± 0.010
28	NGC 6681	-1.35 ± 0.03	2.0	19.25 ± 0.09	0.690 ± 0.007	15.70 ± 0.05	3.55 ± 0.10	0.282 ± 0.011
29	NGC 6723	-0.96 ± 0.04	2.6	19.00 ± 0.09	0.725 ± 0.007	15.45 ± 0.05	3.55 ± 0.10	0.271 ± 0.011
30	NGC 6752	-1.24 ± 0.03	5.3	17.35 ± 0.08	0.705 ± 0.005	13.80 ± 0.10	3.55 ± 0.13	0.270 ± 0.010
31	NGC 6779	-1.61 ± 0.13^{b}	9.5	19.80 ± 0.11	0.840 ± 0.008	16.30 ± 0.05	3.50 ± 0.12	0.290 ± 0.012
32	NGC 6809	-1.54 ± 0.03	3.9	17.95 ± 0.12	0.680 ± 0.014	14.45 ± 0.10	3.50 ± 0.16	0.279 ± 0.018
33	NGC 6838	-0.73 ± 0.03	6.7	17.95 ± 0.06	0.935 ± 0.005	14.50 ± 0.05	3.45 ± 0.08	0.301 ± 0.008
34	NGC 7078	-2.02 ± 0.04	10.3	19.25 ± 0.06	0.650 ± 0.004	15.90 ± 0.05	3.35 ± 0.08	0.295 ± 0.007
35	Pal 12	-0.83 ± 0.06	16.2	20.35 ± 0.06	0.695 ± 0.005	17.18 ± 0.02	3.17 ± 0.06	0.356 ± 0.007

[a] From Carretta & Gratton 1997.

[b] From Zinn & West 1984 (transformed to the Carretta & Gratton 1997 scale, as given by Carretta & Gratton 1997).

though the photometric calibration has been accomplished using the same set of standards (Landolt 1992) and at the same level of accuracy. Figure 1 is an example of our photometry. The CMDs of four clusters, representing diagrams covering the whole range in quality of our data, are shown.

3. METHODOLOGY

A key point of the present analysis is the totally homogeneous photometric sample that has been obtained. There are several other improvements with respect to previous investigations. In particular, (1) we have used and analyzed three of the most recent evolutionary models; (2) the theoretical trends of the photometric parameters have been modeled with third-order polynomials in both age and metallicity instead of with straight lines; and (3) a new and more homogeneous metallicity scale (0.05 dex is the typical internal error on [Fe/H]), calibrated on a large homogeneous spectroscopic sample, has been used. We now discuss how the two observational databases were used to define our differential age estimators and how the theoretical models were parameterized in order to convert our parameters into relative ages.

3.1. Differential Age Estimators

Recent discussions of the possible choices for the photometric parameters (which always measure the TO position with respect to some other CMD feature with negligible dependence on age) can be found in S96, Sarajedini et al. (1997), and B98. Our investigation is based on two "classical" reddening- and distance-independent parameters: the magnitude difference ΔV_{TO}^{HB} between the HB and the TO (vertical method) and the color difference $\delta(V-I)_{2.5}$ between the TO and the RGB (horizontal method), where the RGB color is measured 2.5 mag above the TO. These quantities are displayed in Figure 2 for NGC 1851.

A few other parameters, introduced in previous works, have been measured and tested. V90 were the first to suggest that the point on the main sequence (MS) 0.05 mag redder than the TO could be a better vertical reference point than the TO itself. This point has been consequently used for analyzing the magnitude difference relative to the HB level (B98) and as a reference point for measuring the RGB-TO color difference 2.5 mag above it (V90). We found this point useful for the very best diagrams ($\sim$10 in our sample), but it is very difficult or impossible to measure it
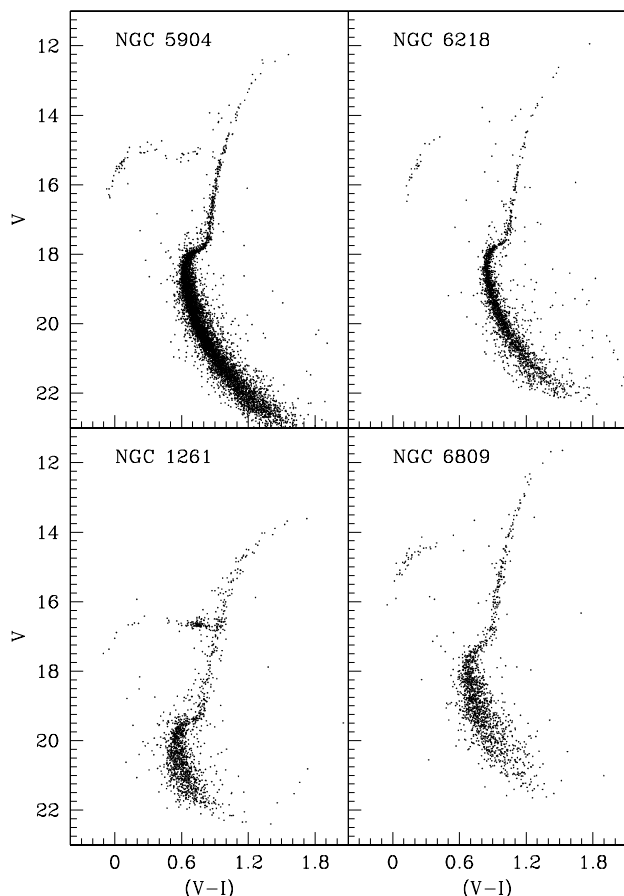
FIG. 1.—CMDs of four clusters used in the relative-age determination, which show the range in quality that is spanned by the present data set. *Top*, two of the best CMDs (for the clusters NGC 5904 and NGC 6218); *bottom*, NGC 6809 and NGC 1261 are an example of lower quality photometric samples. In each case, the HB is populated by a good number of stars, and more than 1 mag below the TO is covered even in the case of NGC 1261.
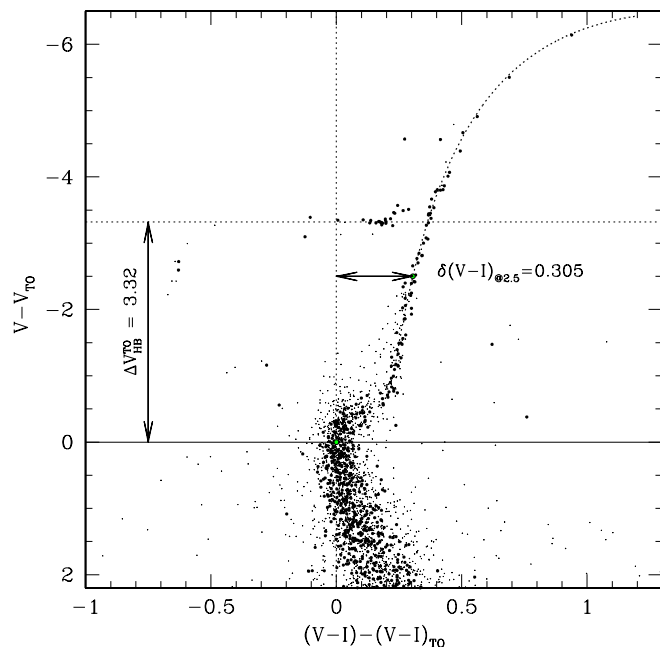

FIG. 2.—CMD of NGC 1851. The heaviest points represent the selected CMD used to measure the TO position and to fit the RGB fiducial line. Magnitude and color have been registered to the TO point. The vertical ΔV_{TO}^{HB} and horizontal $\delta(V-I)_{2.5}$ parameter values for this cluster are indicated by arrows. The analytical fit to the RGB is also shown.

for $\sim 50\%$ of our clusters. Indeed, we must recall that, from the observational point of view, we had to reach a compromise between the deepness of our photometry and the size of the sample that we could collect with a 1 m–class telescope. As a result, while the TO position can be reliably measured for all of our selected clusters, the "0.05" point (which is ~ 1 mag fainter than the TO) generally falls in an MS region where the photometric scatter is larger.

One might also question the $\Delta V = 2.5$ mag choice and whether a brighter point on the RGB would be better. To this, we must consider that as we go from the TO up to the brighter part of the RGB, the photometric error becomes smaller, but the RGB dependence on [Fe/H] gets larger. At the same time, the RGB is less and less populated, so that it can be defined with a lower accuracy. In any case, we made some tests by measuring the TO-RGB color difference for magnitude offsets ranging from 1.5 to 3.5 mag above the TO. We concluded that the $\delta(V-I)_{2.5}$ parameter represents the best compromise.

3.2. *Measurement Procedures*

In order to measure the morphological parameters, first the fiducial MS lines were found by taking the median of the color distributions obtained in magnitude boxes that contain a fixed number of stars, ranging from 50 to 200

stars. The actual number was a function of the total number of stars observed in the cluster. This method allows us to adapt the height of the magnitude box to the number of stars that are found in each branch. It has the advantage, for example, that the TO region, which has a strong curvature, can be sampled with a small magnitude bin (0.03 or 0.04 mag, typically).

The RGBs were defined by fitting an analytic function to the fiducial points, starting from ~ 1 mag in V above the TO. We found that a hyperbolic function gives an excellent fit to these regions, being able to follow the RGB trend even for the most metal-rich clusters (Saviane et al. 1999b). In particular, a function of the form

$$V = a + b(V-I) + c/[(V-I) - d]$$

was used. A dotted line shows the fit to the NGC 1851 RGB in Figure 2.

The HB level was found from the actual HB star distribution for each cluster, by comparison with an empirically defined fiducial HB. The latter was defined by starting with a bimodal HB cluster (NGC 1851) and extending the HB to the red and to the blue by using our best metal-rich and metal-poor clusters, respectively. Once the best fit was found, the value V_{HB} was read at a color that corresponds to $V - I = 0.2$ on the fiducial HB.

Finally, the TO position was found in a two-step procedure. First, a preliminary location was defined by taking the color and the magnitude of the bluest point on the fiducial MS lines; then the color was fine-tuned by computing statistics of the color distribution near this point. All fiducial points whose colors are within ± 0.01 mag of this preliminary TO position estimate were used to compute the mean value that was assigned to the TO. This step was iterated 20 times, keeping the color box fixed but changing

each time the stars that actually enter into the statistical computation, according to the TO position. Usually, the procedure converges very quickly.

The measured values for the 35 GGCs are presented in Table 1. The TO magnitudes and colors are given in columns (5) and (6), while the obtained HB level is given in column (7).

3.3. *Observational Errors*

In order to estimate the uncertainty in the adopted TO color and magnitude, we built a few hundred synthetic CMDs for each cluster, using the Padova library of isochrones (see Bertelli et al. 1994). These CMDs were constructed by adopting for each cluster the corresponding metallicity, the photometric errors (as estimated from the star dispersion along the MS and lower subgiant branch [SGB]), and the total number of stars in the observed CMD. Each synthetic model corresponding to a given cluster was computed with the same input parameters, varying only the initial random number generator seed. The procedure used to determine the TO (see § 3.2) was repeated for the synthetic diagrams associated with each cluster, and the standard deviation of the results was assumed to be the errors actually affecting the color and magnitude of the TO in the observed CMDs.

The errors on the HB level are more difficult to estimate. As explained before, the HB level was found by using an empirically defined fiducial HB. The usually small number of stars in this branch and their nonlinear distribution with magnitude or color (from totally red HBs to nearly vertical blue HBs) do not allow an easy estimate of the uncertainty associated with the HB magnitude. The errors have been estimated by allowing the empirically defined fiducial HB to move from the upper to the lower envelope of the HB in each cluster. The uncertainties obtained in this way turned out to be similar among the clusters with red HBs and among the clusters with blue HBs. Therefore, we decided to use a mean error of ~ 0.05 mag for the red HB objects and of ~ 0.10 mag for the blue ones. Note that these uncertainties must be considered an upper value for the error, as among the stars in the brighter HB envelope there are surely evolved HB stars. Our HB-level estimates are always within 0.1 mag of the Harris (1996) compiled values, with the exception of four clusters (NGC 6779, 6681, 6093, and 6254) for which more recent published photometry is found to be in better agreement with our estimates than with Harris (1996).

The estimated error for the RGB colors is the standard deviation of the distribution of the residuals from the fiducial RGB of the color of the stars located between 1.5 and 3.5 mag above the TO. The final error on $\Delta V_{\mathrm{TO}}^{\mathrm{HB}}$ is obtained as the quadratic sum of the errors on the TO and HB magnitudes, while the error on $\delta(V-I)_{2.5}$ considers both the error in color and magnitude of the TO (which affects the position of the reference point on the RGB), and the error on the color of the point 2.5 mag brighter than the TO magnitude.

3.4. *Theoretical Models*

In order to interpret the results of our data samples, the theoretical isochrones computed by Straniero, Chieffi, & Limongi (1997, hereafter SCL97), Cassisi et al. (1998, hereafter C98), and VandenBerg et al. (1999, hereafter V99) were used. These isochrones are the most recent ones that

provide $V - I$ colors and use updated physics. It is important to note that these theoretical models are completely independent: indeed, they are obtained with different prescriptions for the mixing-length parameter, the Y versus Z relation, the temperature-color transformations and bolometric corrections, etc. The differences among the relative ages resulting from the models can be taken as an indication of the (internal) uncertainties intrinsic to our present knowledge of the stellar structure and evolution. The same morphological parameters already defined for the observational CMDs were measured on the isochrones.

The trends of the theoretical quantities as functions of both age and metallicity were least-squares interpolated by means of third-order polynomials, such that the observed parameters can be easily mapped into age and metallicity variations. The details of the fitting relations are reported in Appendix A.

In order to calculate the theoretical values of $\Delta V_{\mathrm{TO}}^{\mathrm{HB}}$, we have to assume a relation for the absolute V magnitude of the HB as a function of the metal content. In particular, here we adopted $M_V^{\mathrm{ZAHB}} = 0.18([\mathrm{Fe/H}] + 1.5) + 0.65$, from the recent investigation of Carretta et al. (1999). The implications of this choice will be discussed in the following sections.

4. CLUSTERS' RELATIVE AGES

In this section, relative ages are obtained from the observed $\Delta V_{\mathrm{TO}}^{\mathrm{HB}}$ and $\delta(V-I)_{2.5}$ parameters by comparison with the V99 and SCL97 models. As discussed in the § 1, from the observational point of view, the horizontal method is a more precise relative-age indicator than is the vertical one (SD90; V90), as further demonstrated in § 5. Unfortunately, the dependence of RGB temperature on the adopted mixing-length parameter (whose dependence on metallicity is not well established yet) and the uncertain run of the alpha-element enhancement and helium content with the metallicity (which affect the vertical method as well) make the data interpretation not straightforward. A detailed analysis of these effects is beyond the purpose of the present paper. However, we made an internal consistency check for the theoretical models and selected those for which the relative age trend with metallicity turned out to be same (within the errors), using both the horizontal and vertical methods. While the V99 and SCL97 models satisfy this condition (see Figs. 3 and 4) for our sample of GGCs, the C98 models do not. Further tests are required to identify the source of this problem, but it could be possibly related to the I bolometric corrections (see Appendix B), so the C98 model predictions might still be valid for the V and B bands. In any case, because of this internal inconsistency, from here on we will base our analysis on the V99 and SCL97 models only. The implications of the comparison between the observed data and the C98 models are presented in Appendix B.

We want to note that the *absolute* ages obtained from the two methods are not the same. The age differences between the vertical and horizontal methods are ~ 1.2 and ~ 1.5 Gyr for the SCL97 and V99 models, respectively. This discrepancy can be removed by adopting an appropriate constant for the V_{HB} versus [Fe/H] relation. Far from being a problem for our purpose of measuring relative ages, these discrepancies can be a way to test the models and to fine-tune some still-uncertain input parameters. These points are further discussed in Appendix B.
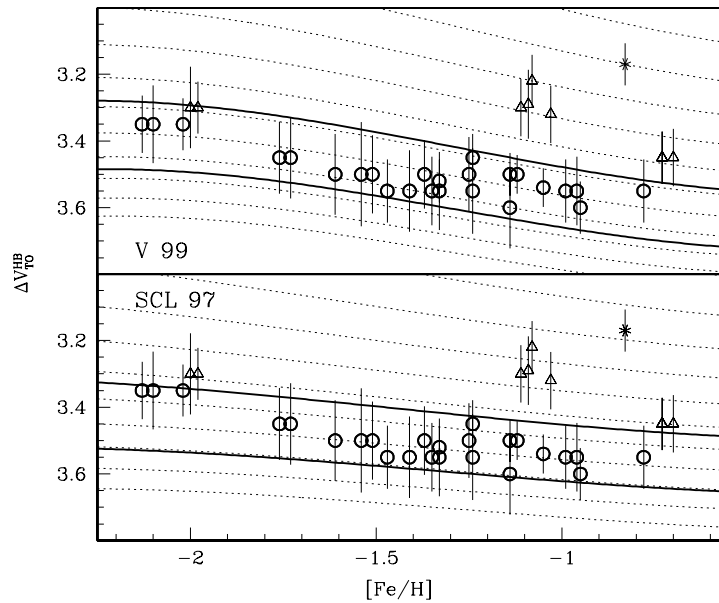
FIG. 3.—Measured $\Delta V_{\rm TO}^{\rm HB}$ parameter plotted vs. the metallicity. The dotted lines in the two panels show the theoretical trend for V99 (*top*) and SCL97 (*bottom*) models. The isochrones are spaced by 1 Gyr (starting from 18 Gyr at the bottom). The asterisk represents the cluster Pal 12. The two isochrones displayed as solid lines represent the ± 1 standard deviation limits of the $\Delta V_{\rm TO}^{\rm HB}$ parameter for the entire sample (excluding Pal 12), and clusters falling within these (*circles*) are defined as " fiducial coeval " clusters. Note that the two independent models give the same fiducial coeval object selection.

4.1. Ages from the Vertical Method

The measured $\Delta V_{\rm TO}^{\rm HB}$ parameter (and the corresponding error) is listed for each cluster in Table 1 (col. [8]). These values are plotted versus the cluster metallicity in Figure 3. The dotted lines are the isochrones from the V99 (*top*) and the SCL97 (*bottom*) models. Age is spaced by 1 Gyr steps, with the lowermost line corresponding to 18 Gyr.

We note in Figure 3 that the clusters are distributed in a narrow band of ≤ 2 Gyr width, apart from five clusters at [Fe/H] values between -1.1 and -0.8 (namely, NGC 2808, 362, 1261, and 1851 and Pal 12). Within the observational errors, the theoretical isochrones and the observed values show similar trends with metallicity for [Fe/H] ≤ -0.9. It must be stated that this result depends
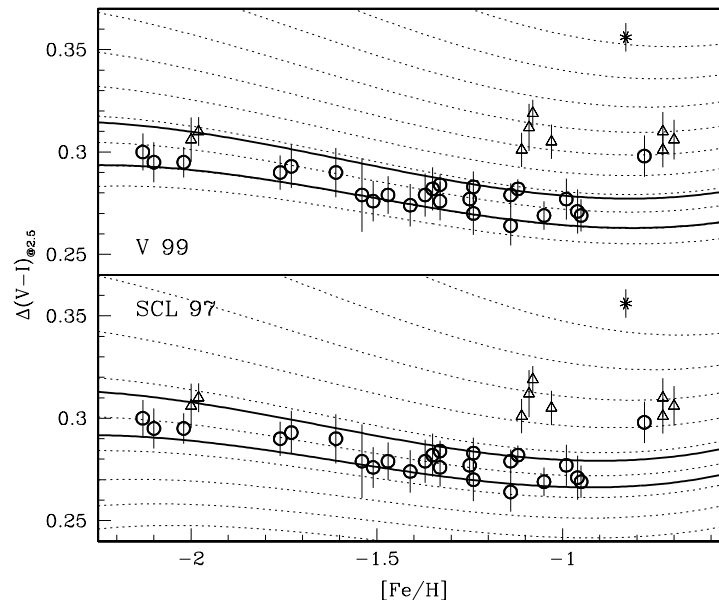

FIG. 4.—Measured $\delta(V-I)_{2.5}$ parameter plotted vs. metallicity. The same two sets of theoretical models of Fig. 3 are shown (*dotted lines*). Age is spaced in 1 Gyr steps, the bottommost line corresponding to 18 and 17 Gyr isochrones, for V99 and SCL97, respectively. The fiducial coeval clusters selected in Fig. 3 are plotted as open circles. The two isochrones displayed as solid lines represent the ± 1 standard deviation limits of the $\delta(V-I)_{2.5}$ parameter for the GGC sample (except Pal 12). Notice that the two clusters at [Fe/H] $= -0.73$ (NGC 6366 and NGC 6838) have the same $\Delta V_{\rm TO}^{\rm HB}$, so they appear as a single point in Fig. 3.

on the choice of the trend of the HB luminosity with [Fe/H], although the conclusions would be the same if the slope of the V_{HB} versus [Fe/H] relation were changed by no more than $\pm 15\%$ (see Fig. 3; *bottom*). There is also a small second-order dependence of the relative ages on the zero point of the relation, but this just changes all the relative ages by a constant factor, while the trend with [Fe/H] remains unchanged.

The isochrones were used to tentatively select a sample of coeval clusters. First, for each stellar evolution library, the theoretical locus that best fitted the sample (not including Pal 12) was found and the relative ΔV_{TO}^{HB} with respect to this locus was computed. We then chose to define as coeval GGCs those clusters whose vertical parameter was within ± 1 standard deviation from the best-fitting isochrone. This interval is marked by thick lines in Figure 3. Objects lying within this interval for both sets of theoretical models (which we will call "fiducial coeval" clusters from here on) are marked by open circles in Figure 3 and will be used later to test the isochrones in the $\delta(V-I)_{2.5}$ versus [Fe/H] plane. Interestingly enough, the same set of coeval clusters is selected using both the SCL97 and V99 isochrones and using any slope α for the V_{HB} versus [Fe/H] relation in the range $0.17 < \alpha < 0.23$ for the V99 isochrones and $0.15 < \alpha < 0.20$ for the SCL97 isochrones. The best-fitting isochrones have ages of 14.3 Gyr, according to the V99 models, and 14.9 Gyr, according to the SCL97 ones. As discussed below, the actual dispersion of the fiducial coeval clusters around the mean isochrone is indeed consistent with a null age dispersion.

We now turn our attention to those clusters that depart from the distribution of the fiducial coeval clusters. It must be noted that the discrepancies are always in the sense of younger ages (smaller ΔV_{TO}^{HB}); moreover, for the discrepant clusters at [Fe/H] ≤ -0.9, there are counterparts with similar metallicity within the coeval sample, whereas for the more metal-rich clusters the situation is less clear. Indeed, if we rely on the theoretical models, the three most metal-rich clusters would seem younger than 47 Tuc. However, it is well known that problems arise in modeling the RGB of metal-rich stars (e.g., S96), so it could also be the case that the coeval cluster band actually turns up at the metal-rich end more than is predicted by the adopted models. We will have to come back to this point later.

For a better comparison of the results from the two methods, we calculated what we call the mean normalized age. First, we derived the best mean age of the "coeval" clusters, according to each of the two sets of evolutionary models: viz., 14.3 Gyr for V99 and 14.9 Gyr for SCL97. Then, for each cluster, we calculated the ratios of the actual age for that cluster (as deduced from the model grids in the two panels of Fig. 3; see Appendix A) relative to the mean age, for the two cases. The mean of these two normalized ages is listed in column (3) of Table 2. The errors are the age intervals covered by the photometric error bars in the normalized age scale. In addition, column (4) of the Table 2 gives the difference between the absolute mean age of each cluster and the absolute age of the bulk of the GGCs, assuming that the latter is 13.2 Gyr as in Carretta et al. (1999).

The age dispersions resulting from the vertical method are ± 1.4 Gyr (independent of the adopted model) when using the entire sample (excluding Pal 12); when only the fiducial coeval sample is considered, the age dispersions

become ± 0.7 and ± 0.6 Gyr, using the SCL97 and V99 models, respectively. In terms of percent values, this translates into a 9.2% and 9.8% (all clusters minus Pal 12) and 4.4% and 4.5% (coeval sample) age dispersion. These latter dispersions are fully compatible with the uncertainties in the ΔV_{HB}^{TO} values, strengthening the idea that the clusters selected as coeval must indeed have the same age.

4.2. *Ages from the Horizontal Method*

The measured $\delta(V-I)_{2.5}$ parameters are presented in Table 1 (col. [9]) and plotted versus the cluster metallicity in Figure 4. The dotted lines in the figure represent the isochrones from V99 (*top*) and SCL97 (*bottom*), in 1 Gyr steps. The bottommost lines are the 18 and 17 Gyr isochrones from V99 and SCL97, respectively.

Remarkably enough, Figure 4 resembles Figure 3: again, most clusters are located in a narrow sequence for [Fe/H] ≤ -0.9, with the exception of the same five clusters identified previously, which also have younger ages in this case. Also, the trend with metallicity is conserved, with a similar uprise at the metal-rich end. For the clusters at [Fe/H] ≤ -0.9 dex, the run of $\delta(V-I)_{2.5}$ is also reproduced by the isochrones. In this metallicity range, the clusters selected as fiducial coeval by the vertical method (Fig. 4, *open circles*) still fall within a chronologically narrow band of ≤ 2 Gyr, showing a remarkable consistency between the two methods.

Apparently, the more metal-rich clusters are younger than the bulk of GGCs. Once more, this result is totally model dependent, and we must recall again that uncertainties in the color-temperature relations and mixing-length calibration, as well as the run of the alpha elements' content and helium abundance with metallicity, could affect the relative ages obtained for the most metal-rich objects (e.g., S96). Therefore, a problem with the theoretical relations cannot be excluded, and NGC 104, 6366, 6352, and 6838 could indeed be coeval with the other clusters. Nevertheless, it must be noted that the same trend is present in ages from the vertical method. Moreover, if we apply a 0.07 mag correction for the HB magnitude of the four most metal-rich clusters (as suggested by B98), the ages obtained from the vertical method would be shifted toward lower values, making them perfectly consistent with the results from the horizontal method. It is therefore tempting to consider the age trend for the metal-rich clusters to be a real possibility (which must be further tested with independent methods), although the precise age offset remains to be established. In any case, if we take the metal-rich clusters as a single group, their internal age dispersion is comparable to that of the rest of the fiducial coeval clusters.

As for the vertical method, normalized ages were obtained by means of the difference in the $\delta(V-I)_{2.5}$ parameter with respect to the best-fitting isochrones (13.1 and 16.4 Gyr for the SCL97 and V99 models, respectively). The resulting values are listed in Table 2 (cols. [5] and [6]). In the table, the normalized ages (col. [5]) are the mean of the two values obtained using the two models, while the age deviations in Gyr given in column (6) are computed from column (5), assuming (as was done in § 4.1) a mean absolute age of 13.2 Gyr (Carretta et al. 1999) for the mean age of the GGC bulk. The errors are the age intervals covered by the photometric error bars in the normalized age scale.

Since the $\delta(V-I)/\delta t$ relation depends on the metallicity in a nonlinear way, the width covered by the ± 1 standard

TABLE 2

RELATIVE AGES OF GGCs

CLUSTER (1)	OTHER ID (2)	VERTICAL METHOD (Gyr)		HORIZONTAL METHOD (Gyr)		MEAN AGE (Gyr)		RELATIVE AGE (9)
		$\overline{\text{Age}}$ (3)	ΔAge (4)	$\overline{\text{Age}}$ (5)	ΔAge (6)	$\overline{\text{Age}}$ (7)	ΔAge (8)	
NGC 104	47 Tuc	0.97 ± 0.10	-0.4 ± 1.4	0.84 ± 0.07	-2.0 ± 0.9	0.90 ± 0.08	-1.2 ± 1.2	Y (?)
NGC 288	...	0.97 ± 0.07	-0.3 ± 0.9	0.97 ± 0.04	-0.3 ± 0.5	0.97 ± 0.05	-0.3 ± 0.7	C
NGC 362	...	0.77 ± 0.10	-2.9 ± 1.4	0.77 ± 0.07	-2.9 ± 1.0	0.77 ± 0.08	-2.9 ± 1.2	Y
NGC 1261......	...	0.72 ± 0.08	-3.6 ± 1.0	0.74 ± 0.04	-3.3 ± 0.5	0.73 ± 0.05	-3.5 ± 0.8	Y
NGC 1851......	...	0.79 ± 0.09	-2.7 ± 1.2	0.80 ± 0.06	-2.5 ± 0.7	0.80 ± 0.07	-2.6 ± 0.9	Y
NGC 1904......	M79	1.00 ± 0.11	0.0 ± 1.4	1.00 ± 0.07	0.0 ± 0.9	1.00 ± 0.08	0.0 ± 1.2	C
NGC 2808......	...	0.78 ± 0.09	-2.8 ± 1.2	0.83 ± 0.05	-2.1 ± 0.7	0.81 ± 0.07	-2.5 ± 0.9	Y
NGC 3201......	...	0.93 ± 0.07	-0.8 ± 1.0	0.96 ± 0.05	-0.4 ± 0.7	0.95 ± 0.06	-0.6 ± 0.8	C
NGC 4590......	M68	0.90 ± 0.11	-1.2 ± 1.5	0.97 ± 0.06	-0.3 ± 0.7	0.94 ± 0.08	-0.8 ± 1.1	C
NGC 5053......	...	0.90 ± 0.07	-1.2 ± 1.0	0.95 ± 0.04	-0.6 ± 0.5	0.93 ± 0.05	-0.9 ± 0.7	C
NGC 5272......	M3	1.01 ± 0.07	0.1 ± 0.9	0.97 ± 0.03	-0.3 ± 0.4	0.99 ± 0.05	0.0 ± 0.7	C
NGC 5466......	...	0.95 ± 0.08	-0.6 ± 1.1	1.01 ± 0.05	0.1 ± 0.6	0.98 ± 0.06	-0.2 ± 0.8	C
NGC 5897......	...	1.00 ± 0.12	0.0 ± 1.6	1.00 ± 0.06	0.0 ± 0.8	1.00 ± 0.09	0.0 ± 1.2	C
NGC 5904......	M5	0.96 ± 0.06	-0.4 ± 0.8	0.95 ± 0.03	-0.6 ± 0.4	0.96 ± 0.04	-0.5 ± 0.6	C
NGC 6093......	M80	1.06 ± 0.10	0.8 ± 1.3	1.02 ± 0.06	0.3 ± 0.8	1.04 ± 0.07	0.5 ± 1.0	C
NGC 6121......	M4	1.01 ± 0.06	0.0 ± 0.8	1.02 ± 0.05	0.3 ± 0.7	1.01 ± 0.05	0.1 ± 0.7	C
NGC 6171......	M107	1.04 ± 0.09	0.5 ± 1.1	1.01 ± 0.06	0.1 ± 0.8	1.02 ± 0.07	0.3 ± 0.9	C
NGC 6205......	M13	1.04 ± 0.12	0.5 ± 1.6	1.01 ± 0.06	0.1 ± 0.8	1.02 ± 0.09	0.3 ± 1.2	C
NGC 6218......	M12	1.07 ± 0.13	0.9 ± 1.7	1.07 ± 0.07	0.9 ± 0.9	1.07 ± 0.10	0.9 ± 1.3	C
NGC 6254......	M10	0.98 ± 0.12	-0.2 ± 1.5	1.00 ± 0.06	0.0 ± 0.8	0.99 ± 0.08	0.0 ± 1.2	C
NGC 6341......	M92	0.95 ± 0.11	-0.6 ± 1.4	1.03 ± 0.05	0.4 ± 0.7	0.99 ± 0.08	0.0 ± 1.1	C
NGC 6352......	...	0.86 ± 0.09	-1.7 ± 1.2	0.78 ± 0.07	-2.8 ± 0.9	0.82 ± 0.08	-2.3 ± 1.1	Y (?)
NGC 6362......	...	1.00 ± 0.10	0.0 ± 1.4	0.97 ± 0.07	-0.3 ± 0.9	0.99 ± 0.08	-0.1 ± 1.1	C
NGC 6366......	...	0.86 ± 0.09	-1.7 ± 1.1	0.76 ± 0.07	-3.1 ± 0.9	0.81 ± 0.07	-2.4 ± 1.0	Y (?)
NGC 6397......	...	1.00 ± 0.11	0.0 ± 1.4	1.01 ± 0.05	0.1 ± 0.6	1.00 ± 0.07	0.1 ± 1.0	C
NGC 6535......	...	1.02 ± 0.12	0.3 ± 1.6	1.05 ± 0.06	0.7 ± 0.8	1.03 ± 0.09	0.5 ± 1.2	C
NGC 6656......	M22	1.05 ± 0.13	0.7 ± 1.7	1.04 ± 0.07	0.5 ± 0.9	1.04 ± 0.09	0.6 ± 1.3	C
NGC 6681......	M70	1.04 ± 0.11	0.5 ± 1.4	0.99 ± 0.07	0.0 ± 0.9	1.01 ± 0.08	0.2 ± 1.2	C
NGC 6723......	...	0.99 ± 0.11	0.0 ± 1.5	1.00 ± 0.09	0.0 ± 1.0	1.00 ± 0.09	0.0 ± 1.3	C
NGC 6752......	...	1.03 ± 0.14	0.4 ± 1.8	1.04 ± 0.07	0.5 ± 1.0	1.03 ± 0.10	0.5 ± 1.4	C
NGC 6779......	M56	1.03 ± 0.12	0.4 ± 1.6	0.99 ± 0.07	0.0 ± 1.0	1.01 ± 0.09	0.1 ± 1.3	C
NGC 6809......	M55	1.02 ± 0.16	0.3 ± 2.1	1.04 ± 0.11	0.4 ± 1.5	1.03 ± 0.13	0.4 ± 1.8	C
NGC 6838......	M71	0.86 ± 0.09	-1.7 ± 1.1	0.81 ± 0.06	-2.4 ± 0.8	0.84 ± 0.07	-2.1 ± 1.0	Y (?)
NGC 7078......	M15	0.94 ± 0.07	-0.7 ± 1.0	1.02 ± 0.04	0.3 ± 0.5	0.98 ± 0.05	-0.2 ± 0.8	C
Pal 12	...	0.65 ± 0.06	-4.5 ± 0.8	0.57 ± 0.04	-5.6 ± 0.6	0.61 ± 0.05	-5.0 ± 0.7	Y

NOTE.—The last column indicates whether the cluster is coeval (C), younger (Y), or probably younger (Y [?]).

deviation limits on the $\delta(V-I)_{2.5}$ parameter (Fig. 4, *solid lines*) is not constant. However, we find that it goes from 0.010 to 0.007 mag for the GGC metallicity range $-2.1 \le [\text{Fe/H}] \le -0.7$. This dispersion is comparable to the experimental mean error for the coeval clusters (0.009 mag; see Table 1).

Using the SCL97 models, the age dispersions that we have from the horizontal method are $\sigma_t = 1.2$ Gyr for the entire sample (with the exception of Pal 12) and $\sigma_t = 0.6$ Gyr (for the fiducial coeval sample), corresponding to a percentage age dispersion of 9.2% and 4.3% for the entire sample and fiducial coeval sample, respectively. Similarly, from the data in Figure 4 (*bottom*), we have $\sigma_t = 1.4$ Gyr and $\sigma_t = 0.6$ Gyr (10.6% and 4.5% for the entire and fiducial coeval samples, respectively). Although the absolute ages of the clusters obtained from each model differ by ~ 3 Gyr, after normalization the relative ages are very similar. Moreover, these relative ages are also close to those given by the vertical method (see § 4.1).

As anticipated in § 1, Figure 4 shows a mild metallicity dependence of the parameter $\delta(V-I)$, smaller than that of

the corresponding parameter $\delta(B-V)$ (B98). Indeed, as shown by SRP97 and confirmed by B98, the slope of the "isochrone" in the [Fe/H], $\delta(B-V)$ plane is $\simeq 0.04$, while if we take the coeval clusters at [Fe/H] < -1 in Figure 4, the slope of the isochrone is approximately -0.025. This means that a typical error of 0.1 dex on the [Fe/H] translates into a ~ 0.4 Gyr error on the relative cluster age if measured using the traditional $B-V$ color, while it yields an error of 0.25 Gyr if the age is measured with the present method.

Moreover, the self-consistency of the ages predicted by the two methods and the two theoretical models strengthens the conclusion by SRP97 that the $\delta(V-I)$ parameter is much more reliable than that of $\delta(B-V)$ as a relative-age index. On the contrary, using $\delta(B-V)$ and totally independent data sets, both Saviane, Rosenberg, & Piotto (1999a) and B98 show that significant discrepancies still exist between the ages predicted by the vertical and horizontal methods.

As stated in § 1, the cluster Pal 12 was included in the present investigation since it provides an excellent reference point for the age calibration. It was found in Paper III that

the age of this cluster is 0.68 ± 0.10 that of both 47 Tuc and M5, as already suggested by Gratton & Ortolani (1988) and Stetson et al. (1989). Here we find that the relative age of Pal 12 with respect to 47 Tuc is 0.68, while it is 0.62 with respect to M5, in agreement with our previous investigation. This result is even more striking if we take into account that our old analysis was based on three other independent models.

5. DISCUSSION: MEAN AGE DISTRIBUTIONS

In this section, the age versus metallicity and Galactocentric distance trends will be discussed. We will use the normalized ages given in columns (3) and (5) of Table 2 for the vertical and horizontal methods, respectively (the mean of these two values is given in col. [7]). Figure 5 plots these normalized ages versus metallicity (*left*) and Galactocentric distance (*right*). We arbitrarily divided our GGC sample into four metallicity groups: (1) the very metal-poor ([Fe/H] < −1.8; *filled circles*), (2) the metal-poor (−1.8 ≤ [Fe/H] < −1.2; *open triangles*), (3) the metal-intermediate (−1.2 ≤ [Fe/H] < −0.9; *filled squares*), and, finally, (4) the metal-rich ([Fe/H] ≥ −0.9; *open diamonds*). Note that Pal 12 is always represented as an asterisk. The values from the vertical (*top*) and horizontal (*bottom*) methods are plotted separately. Figure 5 shows two important features:

The first is that the general trend shown by both methods looks similar (within the errors). A direct comparison of the two methods is provided in Figure 6, where the difference in the normalized relative ages (ΔAge_{vert}^{hor}) is plotted versus the metallicity. There is a very small dispersion of ΔAge_{vert}^{hor} around the zero level in each metallicity group. A marginal offset from the zero level for the two extreme metallicity groups is present. This could arise from discrepancies in the models and/or from the assumed relation for the V_{HB} versus [Fe/H] relation. If we were to act just on the HB level, in order to have the same trend from the two methods, we should use a slope $\Delta M_V^{HB}/\Delta[Fe/H] = 0.08$ or 0.09 for the SCL97 and V99 models, respectively. These values are not consistent with the current estimates of this

slope, so a partial correction of the (theoretical) TO positions should also be considered. At this point, it is very important to remark that the assumptions that must be introduced when using the vertical method are not needed when working with the horizontal one. This method relies on a minimum set of assumptions, thus making the interpretation of the age rankings more straightforward. No parameterization of external quantities (such as the HB magnitude) is required.

The second important point is related to the observational errors. The ΔV_{HB}^{TO} values are affected by uncertainties that are ∼1.5–2.0 times larger than those estimated for the $\delta(V − I)_{2.5}$ parameter. We already commented on the possibility that our errors on ΔV_{HB}^{TO} could be somehow overestimated (and this is also confirmed by the actual dispersion of the points in Fig. 5). On the other side, though the observational errors on $\delta(V − I)_{2.5}$ are surely smaller, we still have to cope with the uncertainty (that we can not estimate) on the theoretical colors when calculating the relative ages with the horizontal method. Still, as the observed trends from both the vertical and horizontal methods are very similar, we prefer to base our further discussion mainly on the results obtained from the horizontal method, where the different trends and effects are more clearly put into evidence. In any case, it must be clearly stated that the discussion would not change using the ages from the vertical method.

5.1. *Distribution in Metallicity*

In Figure 5 (*left*), the fiducial normalized ages are plotted versus the cluster metallicities. Several regions of interest can be discerned in the figure, and as a first step, we discuss here the general trends that can be observed.

The dotted line represents the mean zero relative-age level for the coeval clusters: 26 out of 35 clusters are distributed around the mean within an age interval $\Delta_{age} ≤ 10\%$ of the mean. They all have [Fe/H] < −0.9. In this region, no age-metallicity relation is visible when we take into account
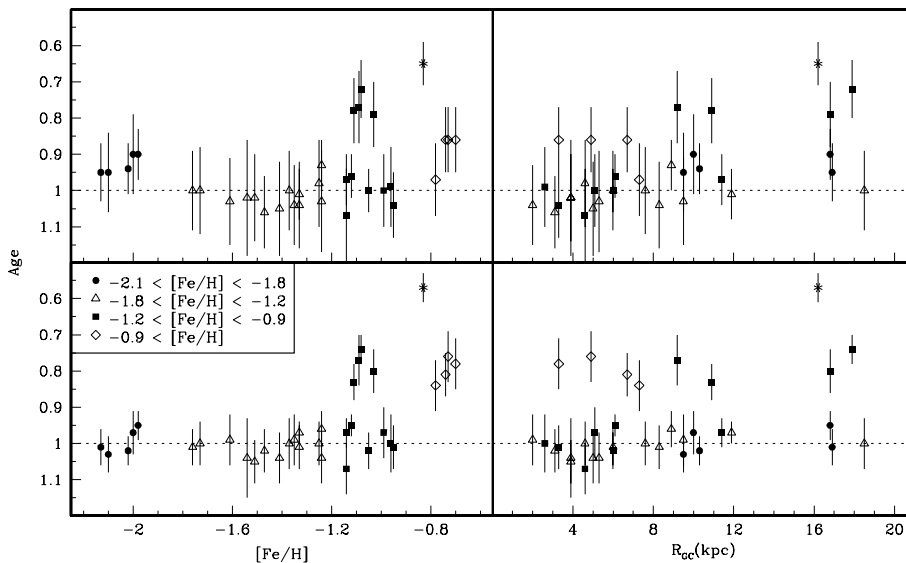

FIG. 5.—Normalized relative ages for our GGC sample from the vertical (*top*) and the horizontal (*bottom*) methods plotted vs. the metallicity (*left*) and vs. Galactocentric distance (*right*). The different symbols represent clusters in different metallicity groups as indicated in the bottom left panel. The error bars are the mean errors as given in cols. (3) and (5) of Table 2. The youngest cluster (*asterisk*) is Pal 12.
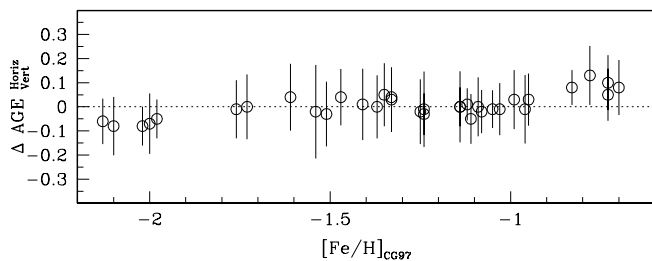
FIG. 6.—Difference in the normalized relative ages obtained from the two methods, $\Delta \mathrm{Age}^{hor}_{vert}$, as a function of the metallicity. The error bars were obtained as the quadratic sum of the errors from the two methods.

the errors on the ages. Within the intermediate-metallicity group, four clusters show definitely younger ages than their equal metallicity counterparts, (namely, NGC 1261, 362, 2808, and 1851). Note also that no younger clusters are detected for $[\mathrm{Fe/H}] < -1.2$.

The five clusters with the highest metallicities in our sample have ages significantly smaller than the mean age distribution. Of these, Pal 12 seems definitely younger than its equal-metallicity counterparts. The remaining four do not show any significant age dispersion. As already discussed in § 4.2, this effect could be due to some problems in the theoretical models at the metal-rich end, but we must note the internal consistency of the two methods. This gives some support to the hypothesis that these four clusters might be really $\sim 17\%$ younger (and Pal 12 $\sim 40\%$ younger) than the bulk of GGCs. These 4 objects are NGC 6366, 6352, 6838, and 104. Note that to assume that these metal-rich clusters are indeed younger would have a strong influence on the Galactic formation scenario, as we discuss in § 6.

Taking the mean normalized ages (Table 2, col. [7]) within the formerly defined metallicity groups, we find for the very metal-poor group a mean normalized age of 0.98 ± 0.03, for the metal-poor group 1.01 ± 0.03, for the metal-intermediate group 0.96 ± 0.12 if the younger clusters are included and 1.00 ± 0.04 if they are not, and for the metal-rich group 0.78 ± 0.10 if Pal 12 is included and 0.83 ± 0.03 if it is excluded. As can be seen, the age dispersion does not vary significantly along the metallicity range if only the coeval clusters are considered. If one includes younger clusters in the computation, then the metal-intermediate group shows a larger age dispersion. This is a well-known property of the GGCs (see, e.g., V90).

In conclusion, our data do not reveal an age-metallicity relation in the usual sense of age decreasing (or increasing) with metallicity. What is found is an increase of the age dispersion (due to the presence of a few clusters with younger ages than the bulk of the GGCs) for the metal-rich clusters, while the lower metallicity ones ($[\mathrm{Fe/H}] \leq -1.2$) all seem to be coeval. This is in agreement with the results of Richer et al. (1996, hereafter R96), Salaris & Weiss (1998, hereafter SW98), and B98. On the other side, Chaboyer, Demarque, & Sarajedini (1996, hereafter C96) proposed an age-metallicity relation, of the order $\Delta t_9/\Delta[\mathrm{Fe/H}] \simeq -4$ Gyr dex^{-1}, which is not present in our data set. What happens for clusters with $[\mathrm{Fe/H}] \geq -0.9$ is totally model dependent; the models suggest a younger age for these objects than for the more metal-poor ones and no age dispersion.

5.2. Testing Young Candidates within Metallicity Groups

In the past, comparisons of relative ages have often been limited to clusters of similar metallicity. This indeed reduces the amount of assumptions to be used and allows an easier check of the relative positions of the fiducial branches of the GGCs. Some "template" globular pairs or groups have many times been used in this exercise. These special comparisons have been done mainly to establish the efficiency of the halo formation, but one could question whether the detection of a single younger cluster can lead to any strong conclusion in favor of some preferred Galactic halo formation model. Aside from this consideration, we want to reexamine here some of the special cases that have drawn much attention in the recent past.

Our checks are made for metallicity groups. Again, the metallicity scale is that of Carretta & Gratton (1997): note that changing the scale would change the absolute values of $[\mathrm{Fe/H}]$ but not the membership in the metallicity groups. For each group, we will consider those clusters that are significantly younger than other members of the same group or those objects that for any reason have received considerable attention in the recent past.

Very low metallicity group ($[\mathrm{Fe/H}] < -1.8$).—For this group, we found no evidence of age dispersion. We will comment on previous investigations (see B98, C96, SW98, V90, and R96) of four globular clusters (GCs) (NGC 4590, 5053, 6341, and 7078). B98 and R96 assign a younger age to NGC 4590, 5053, and 6341, and C96 agree that the former two should be younger. On the other side, SW98 and V90 find that the very metal-poor clusters are all coeval within the errors. Our Table 2 formally indicates that NGC 4590 and 5053 are slightly younger than the other two; however, these differences are smaller than the quoted errors and therefore not significant.

Low-metallicity group ($-1.8 \leq [\mathrm{Fe/H}] < -1.2$).—For this group, we conclude that there is no evidence of age spread. We consider the clusters NGC 5272 (M3), 6205 (M13), and 1904. As in previous studies, we find that M13 is formally older than M3, with NGC 1904 between the two, but these differences are still within the observational errors and therefore not significant. On the contrary, C96 find M13 as much as ~ 2 Gyr older than M3, but the recent accurate photometry of Johnson & Bolte (1998) agrees with our and earlier results.

Intermediate-metallicity group ($-1.2 \leq [\mathrm{Fe/H}] < -0.9$).—For this group, we found clear evidence of age dispersion, with clusters up to $\sim 25\%$ younger than the older members of the group. We will center our attention on NGC 1851, 1261, 288, 2808, and 362. As in the present paper, NGC 2808 has been found to be younger by previous investigations (C96, R96, and B98). NGC 1851 is found to be young by C96, B98, SW98, R96, and the present work, while S96 claim that NGC 1851, 362, and 288 are coeval. NGC 288 and NGC 362 have been often compared in the past: apart from C96, all the previous investigations were based on the CMD obtained by Bolte (1987, 1989). Bolte (1989), C96, R96, V90, and SD90 claim that NGC 362 is significantly younger than NGC 288 (a $\sim 15\%$–20% lower age, in agreement with our result). A different interpretation of the same data is offered by B98 and SW98, who did not find significant age differences. Still, most of the past studies agree with our finding of a somewhat lower age for NGC 362 with respect to NGC 288. In the case of NGC 1261,

apart from C96 (based on Ferraro et al. 1993), past investigations were based on the CMD published by Bolte & Marleau (1989). We find that this cluster is $\sim 25\%$ younger than NGC 288, and this result goes in the same sense of C96, R96, and Bolte (1989), although the size of the age offset is different. In contrast, B98 find no age difference and SW98 find the cluster even older than NGC 288. It is difficult to identify the origin of the difference with respect to the last two investigations, since no value for the age indicators is given by SW98, and B98 use V_{05} as representative of the TO luminosity: since the Bolte & Marleau (1989) CMD becomes quite confused just below the TO level, it is possible that the B98 value is affected by a large error. On the contrary, our CMD is better defined and more populated, allowing a more reliable definition of the fiducial branches. For comparison, our $\Delta V_{0.05}$ estimate would be 0.25 mag brighter than in B98; i.e., we would still find a younger age.

High-metallicity group ([Fe/H] ≥ -0.9).—Except for the case of Pal 12, our conclusion for this group is that these clusters are coeval, within the uncertainties, and possibly younger than the lower metallicity ones. Most previous studies also determined a constant age for this group, with the only exception being C96. For NGC 104 and NGC 6838, all previous studies used the same data sets (i.e., Hesser et al. 1987 and Hodder et al. 1992 for NGC 104 and NGC 6838, respectively), while in the case of NGC 6352, the Fullton et al. (1995) CMD was used by C96 and R96 and that of Buonanno et al. (1999) was used by SW98 and B98. We can therefore take the discrepant C96 result as a sign of the inherent uncertainties of the combined photometric databases and measurement procedures. Indeed, the SW98, B98, and the present study ages, which are based on two independent methods, are all in fairly good agreement.

5.3. Radial Distribution of Age

Some important clues on the Milky Way's formation and early evolution can be obtained from the Galactocentric radial distribution of the GGC relative ages. It is represented in Figure 5 (*right*) and covers the Galactic zone between 2 and 18.5 kpc. The R_{GC} values have been taken from Table 1. We can clearly distinguish two groups of clusters: the old (coeval) ones and a smaller sample of younger clusters. The two groups are better seen in the bottom panel (but see comments on the errors associated with the vertical parameter in § 4.1).

We begin our discussion with those clusters significantly younger than the bulk. They have at least a 10% younger age. Within this group we should distinguish between the "really younger" (NGC 1261, 1851, 2808, and 362 and Pal 12), which have an older counterpart at the same metallicity that turns out to be coeval with most other metal-poor objects, and those lacking an old counterpart with similar metallicity, for which the younger age is deduced by comparison with the models and hence is model dependent (NGC 104, 6352, 6366, and 6838). In the last (most metal-rich) group, four of the five clusters lie within 8 kpc from the Galactic center. A young age for three of them was already suggested by SW98, who find, as we do, an almost null age difference within this group, and an average age $\sim 20\%$ younger than the metal-poor halo clusters. Beyond 8 kpc, five younger clusters are seen in Figure 5, namely, NGC 362, NGC 2808, Pal 12, NGC 1851, and NGC 1261 (in order of increasing R_{GC}).

Coming to the bulk of our cluster sample, we already noticed that for the coeval clusters there is a small age dispersion around the mean zero level ($\sim 4\%$ for the coeval sample), which is consistent with a null dispersion when we take into account the observational errors. This dispersion is much larger if we consider the whole sample, but we do not find any Galactocentric distance versus age relation. However, it is interesting that, if the (uncertain) metal-rich clusters (Fig. 5, *diamonds*) were excluded, it would appear that the age spread increases with the Galactocentric radius. This result has been reached also by R96, C96, SW98, and B98, who include clusters out to 100, 37, 27, and 28 kpc, respectively. All these studies remark that younger clusters are present only in the outer regions.

In summary, the following picture arises from our analysis:

1. According to the current models, most of the clusters are coeval and old.
2. A fraction of the intermediate-metallicity and all the metal-rich clusters (according to the current models) are substantially younger.
3. The younger intermediate-metallicity clusters all have $R_{GC} > 8$ kpc.
4. The young clusters located at larger R_{GC} have typical halo kinematics.

The consequences of these results on the mechanism of halo formation are discussed in the next section.

6. CLUES ON THE MILKY WAY'S FORMATION

Figure 7 shows how the mean normalized relative ages (col. [7] of Table 2) compare with previous large-scale investigations: the different panels show, from top to bottom, histograms of the normalized age distributions found by C96, R96, SW98, B98, and the present study. In order to compare them, they have been normalized to the mean absolute age in each author's scale. For each histogram, the hatched area corresponds to GGCs with a Galactocentric distance smaller than 20 kpc.

It is clear that the age distributions become narrower as we go from older to more recent studies. This is just the sign of the increasing accuracy of the data samples, of the measurement procedures, and of the analysis techniques. The principal improvements that we have introduced are (1) the use of the largest homogeneous CCD database (meaning by homogeneous that the same instrumentation has been used, the same data and photometric reduction procedures have been followed for all clusters, the same calibration standards have been adopted, etc.), (2) the use of two independent methods for the age measurement, (3) the use of VI photometry, and (4) the introduction of a homogeneous metallicity scale and recent theoretical models.

The age-dating progress that has been discussed so far has important consequences on our interpretation of the timescales of the Milky Way's formation. In particular, we go from a halo formation lasting for $\sim 40\%$ of the Galactic lifetime (C96) to the present result of most of the halo clusters being coeval.

Besides this basic result, other clues on the Milky Way's formation have been obtained from the previous discussion. From Figure 5, a chronological order of structure formation can be inferred. The first objects to be formed are the halo clusters. Old clusters are found at any distance from
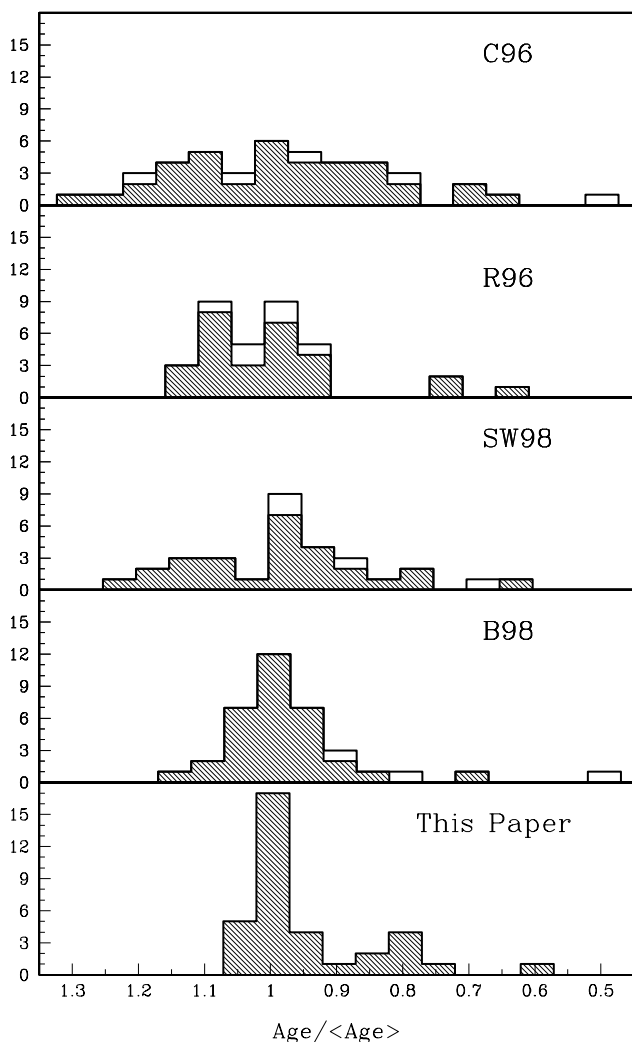
Fig. 7.—Histograms of the relative-age distribution from the most recent compilations in the literature. The histograms are centered on the mean age of the respective samples. Clusters located at the right are younger. The hatched zone represent the clusters within 20 kpc from the center of our Galaxy. The labels identify previous investigations, as explained in the text.

the Galactic center. The GC formation process then started at the same zero age throughout the halo, at least out to ~20 kpc from the center. All the more metal-rich ([Fe/H] ≥ −0.9) clusters formed at later times (~17% of the halo age). Once again, we stress that this interpretation is model dependent, as it depends on the behavior of the isochrones at high metallicities, and it is based on only five objects. Note that these clusters do not identify a unique substructure of the Galaxy. One (Pal 12), likely two (including NGC 6366; see Da Costa & Armandroff 1995), are halo members, one might be a member of the bulge population (NGC 6352; Minniti 1995), and the last two (NGC 6838 and 47 Tuc) of more uncertain classification, either thick-disk members (Armandroff 1989) or halo clusters crossing the disk, following Minniti (1995), who showed that there is no thick-disk GGC population.

Finally, significantly younger halo GGCs are found at any $R_{GC} > 8$ kpc. These clusters (Pal 12 and NGC 1851, 1261, 2808, and 362) could be associated with the so-called

streams, i.e., alignments along great circles over the sky, which could arise from these clusters being the relics of ancient Milky Way satellites of the size of a dwarf galaxy (e.g., Lynden-Bell & Lynden-Bell 1995; Fusi Pecci et al. 1995).

7. CONCLUSIONS

Based on a new large, homogeneous photometric database for 34 Galactic globular clusters (plus Pal 12), a set of distance- and reddening-independent relative-age indicators has been measured. The $\delta(V-I)_{2.5}$ and ΔV_{TO}^{HB} versus metallicity relations have been compared with the relations predicted by two recent updated libraries of isochrones. Using these models and two independent methods, we have found that self-consistent relative ages can be estimated for our GGC sample. In turn, this demonstrates that the two adopted models are internally self-consistent.

Based on the relative age versus metallicity distribution, we conclude that there is no evidence of an age spread for clusters with [Fe/H] < −1.2, all 19 clusters of our sample in this metallicity range being old and coeval. For the intermediate-metallicity group (−1.2 ≤ [Fe/H] < −0.9), there is clear evidence of age dispersion, with clusters up to ~25% younger than the older members. Seven of the 11 GGCs in this group are coeval (also with the previous group), while the remaining four are much younger (namely, NGC 362, 1261, 1851, and 2808). Finally, the metal-rich group ([Fe/H] ≥ −0.9) seems to be coeval within the uncertainties (except Pal 12) and younger (~17%) than the rest of the clusters, this result being model dependent.

From the Galactocentric distribution of the GGC ages, we can divide the GGCs in two groups, the old, coeval clusters and the young clusters. The second group should be divided in two subgroups, the "really young" clusters and the "model-dependent" clusters, located in the intermediate- and high-metallicity groups, respectively. From this distribution, we can present a possible interpretation of the Milky Way's formation:

1. The GC formation process started at the same zero age throughout the halo, at least out to ~20 kpc from the Galactic center.

2. At later (~17% lower) times, the metal-rich GCs were formed (we stress that this interpretation is model dependent).

3. Finally, significantly younger halo GGCs are found at any $R_{GC} > 8$ kpc, for which a possible scenario associated with mergers of dwarf galaxies to the Milky Way could be considered.

APPENDIX A

THEORETICAL MODEL FITTING

As already introduced in § 3.4, and in order to interpret the results of our data samples, the theoretical isochrones computed by SCL97, C98, and V99 were used. On these isochrones, the same morphological parameters already defined for the observational CMDs, $\Delta V_{\rm TO}^{\rm HB}$ and $\delta(V-I)_{2.5}$, were measured.

The trends of the theoretical quantities as a function of both age and metallicity were least-squares interpolated by means of third-order polynomials, so that the observed parameters can be easily mapped into age and metallicity variations. This will allow us to easily translate the parameter values into ages. The equations used are of the form

$$\text{parameter} = a + b[\text{Fe/H}] + c(\log t) + d[\text{Fe/H}]^2 + e(\log t)^2 + f[\text{Fe/H}](\log t)$$
$$+ g[\text{Fe/H}]^3 + h(\log t)^3 + i[\text{Fe/H}]^2(\log t) + j[\text{Fe/H}](\log t)^2 ,$$

where "parameter" represents one of two photometric age indices, $\Delta V_{\rm TO}^{\rm HB}$ or $\delta(V-I)_{2.5}$, and t is the age in Gyr.

The [Fe/H] of the V99 models were provided by the authors, while for the SCL97 and C98 models they were defined as $[\text{Fe/H}] = \log(Z/Z_\odot)$, setting $Z_\odot = 0.02$. The resulting coefficients are listed in Table 3, where the last row also reports the rms of the fits in magnitude and age.

An example of our fits can be seen in Figure 8. The top left panel shows the $\delta(V-I)_{2.5}$ versus $\log(\text{age})$ theoretical behavior (at constant [Fe/H]), while the top right panel shows the same parameter versus [Fe/H] (at constant ages). In both panels, model results are shown by open circles, while our fits are represented by solid lines. In the bottom panels, the absolute residuals of the respective fits are presented. The maximum difference between the model and our fit is 0.006 mag, and the standard deviation ~ 0.0015 mag, which corresponds to 0.15 Gyr. The dotted lines graphically represent these two values.

A second-order polynomial would not be able to follow the theoretical trend of the models, while the distribution of the residuals shows that a fourth order is not required since the residual uncertainty is much smaller than the observational error.

TABLE 3

Coefficients of the Polynomials Used to Interpolate Theoretical Quantities

Coefficient	V99		SCL97		C98	
	$M_V^{\rm TO}$	$\delta(V-I)_{2.5}$	$M_V^{\rm TO}$	$\delta(V-I)_{2.5}$	$M_V^{\rm TO}$	$\delta(V-I)_{2.5}$
a	1.599700	0.828002	−1.580420	0.930417	11.99130	0.667046
b	0.825196	−0.165156	1.111200	−0.356030	2.550110	−0.217992
c	3.801050	−0.812187	12.85960	−1.472910	−23.50860	−0.123297
d	−0.278009	0.191788	−0.226336	0.186956	−0.331870	0.243417
e	−1.428870	0.589075	−10.29670	1.491670	21.91010	−0.008126
f	−1.153670	0.611913	−1.716990	0.970103	−4.612900	0.857613
g	−0.074459	0.021023	−0.025408	0.020722	−0.061030	0.034687
h	0.339905	−0.223764	3.240170	−0.590396	−6.108660	−0.069297
i	−0.007749	−0.077650	0.103320	−0.077396	0.094752	−0.080693
j	0.390382	−0.312448	0.754886	−0.477246	2.124730	−0.421044
rms	0.017 mag	0.002 mag	0.010 mag	0.001 mag	0.017 mag	0.001 mag
	(0.23 Gyr)	(0.15 Gyr)	(0.12 Gyr)	(0.15 Gyr)	(0.20 Gyr)	(0.12 Gyr)

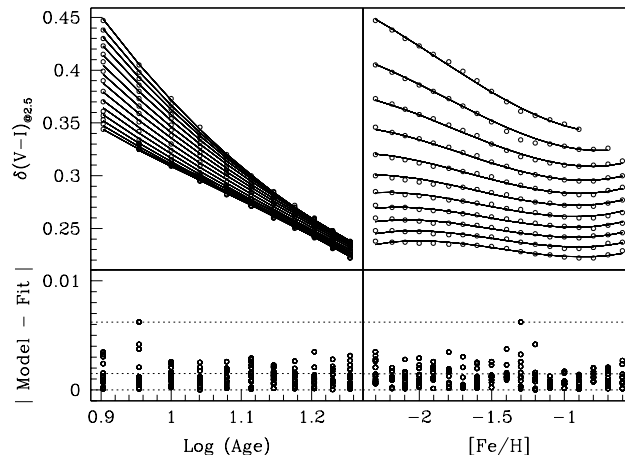
FIG. 8.—Example of our fit to the SCL97 models. The measured values on the theoretical models are fitted in both the $\delta(V-I)_{2.5}$ vs. [Fe/H] plane (top right) and the $\delta(V-I)_{2.5}$ vs. $\log t$ plane (top left). The fits to the theoretical values (open circles) are shown as continuous lines. The bottom panels show the residuals.
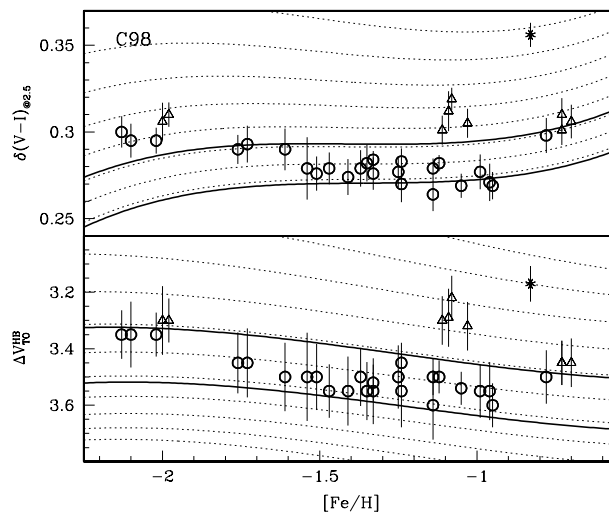
Fig. 9.—Same as Figs. 3 and 4, but for the models of C98

APPENDIX B

A TEST BENCH FOR THE THEORETICAL MODELS

One can look at Figures 3 and 4 as empirical calibrations of the two differential parameters ΔV_{TO}^{HB} and $\delta(V-I)_{2.5}$ as a function of [Fe/H]. Assuming that the two differential parameters are controlled just by the age and the metallicity, when the theoretical loci are superposed on these two diagrams, the same age-metallicity relations must be obtained in the two cases. We have shown that this is true for the SCL97 and V99 models, which indeed yield the same (shallow) age-metallicity relation, both using ΔV_{TO}^{HB} and $\delta(V-I)_{2.5}$.

The same is not true for the C98 models: looking at Figure 9, it is clear that the theoretical isochrones show the same trend seen for the other two sets of models in the bottom panel (vertical method), while, for example, an age-metallicity relation of ~ 5 Gyr dex^{-1} for [Fe/H] < -1 appears when the horizontal parameter is used (inconsistent with the top panel and with what we obtain using SCL97 and V99 models). In order to reconcile the two diagrams, one could play with the HB luminosity-metallicity relation. After a few tests, we found that a partial agreement could be reached by using $M_V^{HB} = 0.35$[Fe/H] $+ 1.40$, but such faint values for the RR Lyrae luminosity are not consistent with the most recent results (see, e.g., Carretta et al. 1999), and the age-metallicity relation would disagree in any case at the high-[Fe/H] end.

We also checked the $B-V$ behavior of the horizontal parameter for the C98 models, and in that case they agree with the SCL97 ones. It is therefore suggested that the problems in the C98 isochrones are related to the I bolometric corrections (which indeed are different from those used by both SCL97 and V99). This test shows how our database can be used to define the useful observational constraints that any model calculation must reproduce. Furthermore, we also suggest that a *multicolor* approach should be followed to fully test the theoretical models.

REFERENCES

Armandroff, T. E. 1989, AJ, 97, 375
Bertelli, G., Bressan, A., Chiosi, C., Fagotto, F., & Nasi, E. 1994, A&AS, 106, 275
Bolte, M. 1987, ApJ, 315, 469
———. 1989, AJ, 97, 1688
Bolte, M., & Marleau, F. 1989, PASP, 101, 1088
Buonanno, R., Corsi, C. E., Pulone, L., Fusi Pecci, F., & Bellazzini, M. 1998, A&A, 333, 505 (B98)
Buonanno, R., et al. 1999, in preparation
Carretta, E., & Gratton, R. G. 1997, A&AS, 121, 95
Carretta, E., Gratton, R. G., Clementini, G., & Fusi Pecci, F. 1999, ApJ, submitted (astro-ph/9902086)
Cassisi, S., Castellani, V., Degl'Innocenti, S., & Weiss, A. 1998, A&AS, 129, 267 (C98)
Chaboyer, B., Demarque, P., & Sarajedini, A. 1996, ApJ, 459, 558 (C96)
Da Costa, G. S., & Armandroff, T. E. 1995, AJ, 109, 2533
Ferraro, F. R., Clementini, G., Fusi Pecci, F., Vitiello, E., & Buonanno, R. 1993, MNRAS, 264, 273
Fullton, L. K., Carney, B. W., Olszewski, E. W., Zinn, R., Demarque, P., Janes, K. A., Da Costa, G. S., & Seitzer, P. 1995, AJ, 110, 652
Fusi Pecci, F., Bellazzini, M., Cacciari, C., & Ferraro F. R. 1995, AJ, 110, 1664
Gratton, R. G., & Ortolani, S. 1988, A&AS, 73, 137

Harris, W. E. 1996, AJ, 112, 1487
Hesser, J. E., Harris, W. E., VandenBerg, D. A., Allwright, J. W. B., Shott, P., & Stetson, P. B. 1987, PASP, 99, 739
Hodder, P. J. C., Nemec, J. M., Richer, H. B., & Fahlman, G. G. 1992, AJ, 103, 460
Johnson, J. A., & Bolte, M. 1998, AJ, 115, 693
Landolt, A. U. 1992, AJ, 104, 340
Lynden-Bell, D., & Lynden-Bell, R. M. 1995, MNRAS, 275, 429
Minniti, D. 1995, AJ, 109, 1663
Richer, H. B., et al. 1996, ApJ, 463, 602 (R96)
Rosenberg, A., Aparicio, A., Saviane, I., & Piotto, G. 1999b, A&AS, submitted (Paper II)
Rosenberg, A., Piotto, G., Saviane, I., & Aparicio, A. 1999a, A&AS, in press (Paper I)
Rosenberg, A., Saviane, I., Piotto, G., Aparicio, A., & Zaggia, S. R. 1998a, AJ, 115, 648
Rosenberg, A., Saviane, I., Piotto, G., & Held, E. V. 1998b, A&A, 339, 61 (Paper III)
Rutledge, A. G., Hesser, J. E., & Stetson, P. B. 1997, PASP, 109, 907
Salaris, M., & Weiss, A. 1998, A&A, 335, 943 (SW98)
Sandquist, E. L., Bolte, M., Langer, G. E., Hesser, J. E., & Mendes de Oliveira, C. 1999, ApJ, 518, 262
Sarajedini, A., Chaboyer, B., & Demarque, P. 1997, PASP, 109, 1321

Sarajedini, A., & Demarque, P. 1990, ApJ, 365, 219 (SD90)
Saviane, I., Rosenberg, A., & Piotto, G. 1997, in Advances in Stellar Evolution, ed. R. T. Rood & A. Renzini (Cambridge: Cambridge Univ. Press), 65 (SRP97)
———. 1999a, in ASP Conf. Ser. 165, The Third Stromlo Symposium: The Galactic Halo, ed. B. K. Gibson, T. S. Axelrod, & M. E. Putman (San Francisco: ASP), 308
Saviane, I., Rosenberg, A., Piotto, G., & Aparicio, A. 1999b, A&A, in press
Stetson, P. B., Hesser, J. E., Smith, G. H., VandenBerg, D. A., & Bolte, M. 1989, AJ, 97, 1360

Stetson, P. B., VandenBerg, D. A., & Bolte, M. 1996, PASP, 108, 560 (S96)
Straniero, O., Chieffi, A., & Limongi, M. 1997, ApJ, 490, 425 (SCL97)
Sweigart, A. V. 1997, ApJ, 474, L23
VandenBerg, D. A., Bolte, M., & Stetson, P. B. 1990, AJ, 100, 445 (V90)
VandenBerg, D. A., Stetson, P. B., & Bolte, M. 1996, ARA&A, 34, 461
VandenBerg, D. A., Swenson, F. J., Rogers, F. J., Iglesias, C. A., & Alexander, D. R. 1999, ApJ, submitted (V99)
Zinn, R., & West, M. J. 1984, ApJS, 55, 45